Microstructure evolution during impact on granular matter

L. Kondic,[1] X. Fang,[1] W. Losert,[2] C. S. O'Hern,[3] and R. P. Behringer[4]
[1]*Department of Mathematical Sciences, New Jersey Institute of Technology, Newark, New Jersey 07102, USA*
[2]*Department of Physics, IPST, and IREAP, University of Maryland, College Park, Maryland 20742, USA*
[3]*Departments of Mechanical Engineering & Materials Science and Physics, Yale University, New Haven, Connecticut 06520-8284, USA*
[4]*Department of Physics and Center for Nonlinear and Complex Systems, Duke University, Durham, North Carolina 27708-0305, USA*
(Received 28 August 2011; published 18 January 2012)

We study the impact of an intruder on a dense granular material. The process of impact and interaction between the intruder and the granular particles is modeled using discrete element simulations in two spatial dimensions. In the first part of the paper we discuss how the intruder's dynamics depends on (1) the intruder's properties, including its size, shape and composition, (2) the properties of the grains, including friction, polydispersity, structural order, and elasticity, and (3) the properties of the system, including its size and gravitational field. It is found that polydispersity and related structural order, and frictional properties of the granular particles, play a crucial role in determining impact dynamics. In the second part of the paper we consider the response of the granular system itself. We discuss the force networks that develop, including their topological evolution. The influence of friction and structural order on force propagation, including the transition from hyperbolic-like to elastic-like behavior is discussed, as well as the affine and nonaffine components of the grain dynamics. Several broad observations include the following: tangential forces between granular particles are found to play a crucial role in determining impact dynamics; both force networks and particle dynamics are correlated with the dynamics of the intruder itself.

DOI: 10.1103/PhysRevE.85.011305 PACS number(s): 45.70.−n, 83.80.Fg, 46.40.Cd, 43.40.+s

I. INTRODUCTION

The problem of impact on a dense granular material has been explored extensively due to its relevance to processes that vary from asteroid impact, numerous technological applications, defense from high speed projectile impact, or to simply walking on a sandy beach. While a large amount of research has been done over hundreds of years, only during the last few decades has significant progress been reached in formulating relatively simple but realistic effective models which characterize the basic features of the interaction between an intruder and a granular material itself.

These effective models have allowed for much better understanding of the dependence of the forces due to impact on various parameters. A simple model due to Poncelet and dating from the 19th century is based on the concept that the force experienced by an intruder may be separated into independent speed- and depth-dependent parts [1]. The speed-dependent part is hydrodynamic-like, while the depth-dependent part is considered to be due to forces of either hydrostatic or frictional origin. While careful experiments [2–9] and simulations [3,10–13] have improved our understanding of the physics of impact considerably, they have also opened a new set of questions. Some of these questions include scaling of the penetration depth with the impact speed and intruder size, for which a variety of sometimes contradictory results exist (see, e.g., [7,8] and discussions therein). The dependence of the granular force on the intruder speed is not always clear [8], and the role of various effects which determine the depth-dependent part of the force is also a subject of discussion, with models that suggest either frictional [10] or hydrostatic-like [13] forces. The picture which has evolved as a result of recent work is that there are multiple regimes where different aspects of the interaction between an intruder and granular particles may be relevant, and it has become obvious that it is necessary to look *into* the granular system itself in order to understand the basic physical mechanisms responsible for determining large scale dynamics of an intruder.

Therefore, in this work we take a different approach by correlating the results for the dynamics of an intruder with the evolution of the microstructure of the granular material itself. In particular, we concentrate on the influence of frictional properties of the granular particles, and on their polydispersity and structural ordering. We show that these quantities may strongly influence the response of the granular material, the interaction between the granular particles and intruder, and, consequently, the dynamics of the intruder itself.

The structure of this paper is as follows. After discussing the simulation techniques in Sec. II, we present in Sec. III results for the intruder dynamics for various parameters characterizing the intruder and the granular system. We compare our results with existing simulations and experiments, with a significant part of this comparison in the Appendix. In the present work we limit ourselves to the regime where the final penetration depth is smaller then or comparable to the intruder size; larger depths will be considered elsewhere. In Sec. IV we then consider the granular material itself. In Sec. IV A we explore properties of the force field, the influence of structural order, polydispersity, and friction on force propagation, and topological quantities describing structure of the force field. In Sec. IV B we discuss affine and nonaffine components of the dynamics of the granular particles. We conclude by discussing the question of energy expenditure, and further elaborate on the role of friction and structural order or granular packing.

II. TECHNIQUES

We consider a rectangular domain in two dimensions with gravity. The particles are polydisperse disks, with

their diameters varying randomly in a range $\pm r$ about the mean. The particle-particle and particle-wall interactions are modeled using the soft-sphere approach that includes friction and rotational degrees of freedom. We solve the following equations of motion for each particle:

$$m_i \frac{d^2\mathbf{r}_i}{dt^2} = \mathbf{F}^n_{i,j} + \mathbf{F}^t_{i,j} + m_i\mathbf{g}, \qquad I_i \frac{d\boldsymbol{\omega}_i}{dt} = -\frac{1}{2} d_i \mathbf{n} \times \mathbf{F}^t_{i,j}. \tag{1}$$

The normal force is given by

$$\mathbf{F}^n_{i,j} = [k_n x - \gamma_n \bar{m} \mathbf{v}_{i,j}]\mathbf{n},$$

where $r_{i,j} = |\mathbf{r}_{i,j}|$, $\mathbf{r}_{i,j} = \mathbf{r}_i - \mathbf{r}_j$, and the normal direction is defined by $\mathbf{n} = \mathbf{r}_{i,j}/r_{i,j}$. The compression is defined by $x = d_{\rm av} - r_{i,j}$, where $d_{\rm av} = (d_i + d_j)/2$, d_i and d_j are the diameters of the particles i and j; $\mathbf{v}^n_{i,j}$ is the relative normal velocity.

The nondimensional force constant k_n is related to the dimensional one k by $k = k_n mg/d$, where m is the average particle mass, d is the average particle diameter, and g is Earth's gravity. All quantities are expressed using d as the length scale, the binary collision time

$$\tau_c = \pi \sqrt{\frac{d}{2gk_n}}$$

as the time scale, and m as the mass scale. Then, $\bar{m}$ is the reduced mass and γ_n is the damping coefficient related to the coefficient of restitution e_n by $\gamma_n = -2 \ln e_n/\tau_c$ (see, e.g., [14]). We take e_n constant and ignore its possible velocity dependence [15]. For definitiveness we typically use the physical parameters that are appropriate for photoelastic disks [16], in particular $d = 4$ mm, $k_n = 4 \times 10^3$, $e_n = 0.5$, although we also consider different values of k_n and e_n. The parameters entering the force model can be connected to the physical properties of the material (Young modulus, Poisson ratio) using the method described, for example, in [14].

Before proceeding with the discussion of the tangential forces, it is appropriate to comment on the presence of two time scales in the problem: one is the fast time scale τ_c, defined above, which is relevant for the processes involving particle collisions, and the other slow penetration time scale is $t_s = \sqrt{D_i/g}$, where D_i is the intruder's diameter. Here t_s is proportional to the time for an intruder to travel a distance equal to its own diameter, starting from rest in a gravitational field. In this work we will concentrate chiefly on the granular dynamics, and therefore τ_c is the most appropriate time scale, and d/τ_c is the most appropriate (fast) velocity scale. The two time scales are related by $\tau_c/t_s = \pi/\sqrt{2D_i k_n} \ll 1$.

The tangential force is specified by two different models, which can be conveniently described within the same framework. The basic approach is based on a Cundall-Strack type of model [17], where a tangential spring of zero length is introduced when a new contact between two particles forms at $t = t_0$. Due to relative motion of the particles, the spring length $\boldsymbol{\xi}$ evolves as

$$\boldsymbol{\xi} = \int_{t_0}^{t} \mathbf{v}^t_{i,j}(t')dt',$$

where $\mathbf{v}^t_{i,j} = \mathbf{v}_{i,j} - \mathbf{v}^n_{i,j}$. For long lasting contacts, $\boldsymbol{\xi}$ may not remain parallel to the current tangential direction defined by $\mathbf{t} = \mathbf{v}^t_{\mathbf{i,j}}/|\mathbf{v}^t_{\mathbf{i,j}}|$ (see, e.g,. [18,19]); we therefore define a corrected $\boldsymbol{\xi}' = \boldsymbol{\xi} - \mathbf{n}(\mathbf{n} \cdot \boldsymbol{\xi})$ and introduce the test force

$$\mathbf{F}^{t*} = -k_t \boldsymbol{\xi}' - \gamma_t \mathbf{v}^t_{i,j},$$

where γ_t is the coefficient of viscous damping in the tangential direction (we use $\gamma_t = \gamma_n/2$). To keep the magnitudes of tangential forces smaller than the Coulomb threshold, specified by $\mu \mathbf{F}^t$, where μ is the coefficient of static friction, we define the tangential force by

$$\mathbf{F}^t = \min(\mu|\mathbf{F}^n|, |\mathbf{F}^{t*}|) \frac{\mathbf{F}^{t*}}{|\mathbf{F}^{t*}|}. \tag{2}$$

In addition, $\boldsymbol{\xi}'$ is reduced to the length corresponding to the value of $|\mathbf{F}^t|$ as needed. This is a commonly used model for static friction, for nonzero k_t. To be able to isolate the effect of static friction, we also consider a commonly used kinetic friction model based on viscous damping, which is obtained simply by putting $k_t = 0$. Therefore, depending on whether static friction effects are considered or not, we use either model 1: $k_t = 0.8k_n$ (the value suggested in [20]), or model 2: $k_t = 0.0$ (kinetic friction only). The exact value of k_t does not seem to be of relevance in the present context as long as $k_t \neq 0$. The particles making up the walls are made very inelastic and frictional, with $\mu = 0.9$ and $e_n = 0.1$.

Figure 1 shows the system setup. Here W and L are the width (depth) and the length of the granular bed, respectively. Periodic boundary conditions are implemented on the left and right boundaries. From below and above, the domain is bounded by rigid horizontal walls made up from monodisperse particles, with the properties as specified above. The role

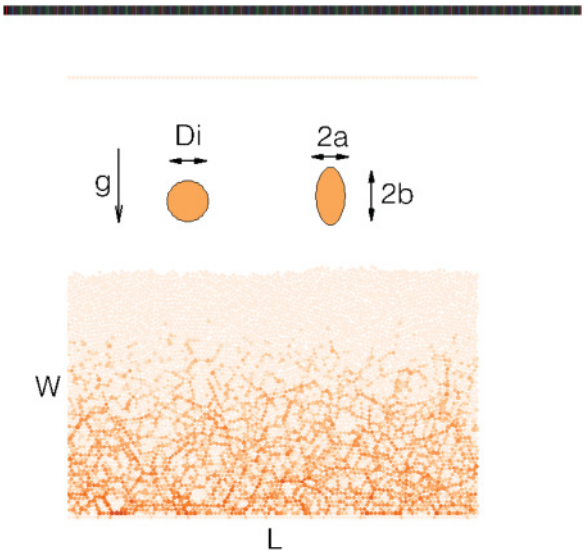

FIG. 1. (Color online) System setup. For illustration we show implementations of both circular and elliptic intruders. In the simulations, one of these shapes is incident on the middle of the upper surface of the granular system. Particles are colored according to the total normal force experienced (here only due to gravity) with dark color showing large force. The intruders' color is for illustration only.

of the top wall is essentially to contain those few particles which would be ejected during particularly violent impacts. However, the upper boundary is positioned sufficiently high that collisions with this wall are very rare.

We consider both circular and elliptical intruders. An elliptical form is one way to represent an ogival shape. The initial height of the intruder is fixed so that the lowest part of the intruder is $5d$ above the granular surface; we then vary the initial intruder's velocity. The implementation of a circular intruder is straightforward. It is still considered to be a single large particle, with is own set of parameters, for example, stiffness, and friction. We model elliptical and ogival intruders as a cluster of 360 granular particles with a mass appropriate to the intruder. This cluster forms a rigid shell on the surface of an ellipse; that is, the particles in the cluster are rigidly attached to each other. In the simulations, the total force on the cluster is computed, and then the positions of all cluster particles are updated by applying Eqs. (1) to the cluster as a whole. We have confirmed that implementing a circular intruder as either a single particle or as a cluster does not influence the results, as discussed below. Although we position the cluster particles on the surface only, we typically consider solid intruders by choosing the cluster moment of inertia appropriately. More precisely, the moment of inertia is given by $I = m_i(a^2 + b^2)/4$, where a and b are the semiaxes of an ogival intruder, and m_i is its mass.

The speed of sound c in the system will be needed below in order to put the results in perspective. We estimate this property by the time needed for information to propagate across the domain. Specifically, we apply a point force at the top of the granular bed and measure the time needed for the force information to reach the bottom. When using the kinetic friction model we find (in dimensionless units) $c \approx 2$, while for the static friction model we find slightly larger $c \approx 2.4$. In our simulations we concentrate on the subsonic regime, and consider intruder speeds up to 1 in our dimensionless units.

In order to examine the effect of the granular microstructure on the impact, we model two types of packings. One is an exact hexagonal lattice with particles of identical size, and the other is a randomly packed system with $r = 0.0$, 0.1, 0.2, 0.3, and 0.4. The hexagonal lattice is prepared by simply positioning the particles so that they initially touch each other, and letting them equilibrate under gravity. The random systems are prepared by positioning the particles on a square lattice, giving them random initial velocities, letting them settle under gravity until the total kinetic energy decays below a given threshold ($10^{-10}mgd_{\mathrm{av}}$), and then smoothing the irregular top surface roughness, if there is any. To consider reproducibility and the influence of a particular configuration on the results, we modify the initial random velocities assigned to the particles, and repeat the simulation.

The simulations are typically carried out using 6000 particles, with the size of the domain in units of the mean particle diameter given by $L = 100$ in the horizontal direction, and the initial height of the granular bed given by $W = 60$, see Fig. 1. After settling, the particles form a system of height $\sim$56 for random polydisperse systems. This system size is at least moderately large. However, to test for system size dependence, we have also carried out simulations in much larger domains containing up to 90 000 particles. The influence of system size on the results is discussed in Sec. III B.

The volume fraction ρ occupied by the grains is difficult to compute precisely due to the presence of a rough (on the grain scale) upper surface. Furthermore, some variations of ρ may also result due to different initial configurations. These variations are less than about 0.01, with typical ρ being in the range 0.85–0.86 for the random polydisperse systems. The influence of the change of simulation parameters, such as polydispersity, force constant, or gravity, leads to modifications of ρ on the same scale as different initial conditions. As we will discuss in the next section, the influence of different initial conditions on large-scale features of the results, such as the final penetration depth, is minor, and therefore we may expect that the influence of slight variations of ρ reported above is not significant. The only case where there is a appreciable difference is the hexagonally ordered system; here $\rho \approx 0.91$, as expected for a lattice compressed under its own weight.

No additional compaction of the granular bed is used; we have experimented with shaking of the bed to increase ρ, however only very minor additional compaction was achieved, and we were not able to quantify its influence on the result that follow. It will be of interest to consider the effect of additional compaction on the intruder's dynamics, perhaps by applying an external load. Another issue which is left for future work is considering the influence of interstitial air on the impact dynamics—in the present work we do not consider this effect.

III. RESULTS FOR THE PENETRATION DEPTH

In this section we discuss results for the penetration depth, and its dependence on parameters characterizing the granular system and of the intruder. We also briefly compare our results to the existing data, with more detailed comparison given in the Appendix. In Sec. IV we discuss the properties of the force field in the system, its dynamics, and its influence on the penetration depth $D(t)$ defined as the distance between the position of the bottom part of the intruder and the initial upper boundary of the granular bed at the point of impact. For the penetration depth measurements, we also calculate the "final" penetration depth $\overline{D}$ by averaging $D(t)$ at long times. Fluctuations in $D(t)$ are typically much smaller than the average particle size.

We start by considering a randomly packed system with particles characterized by polydispersity $r = 0.2$, Coulomb friction $\mu = 0.5$, coefficient of restitution $e_n = 0.5$, and with kinetic friction only $k_t = 0.0$. The intruder is a disk, with diameter of $D_i = 10$ in units of the average particle diameter, and otherwise possessing the same material properties as the granular particles. Figure 2 shows the time evolution of the penetration depths of an intruder impacting the granular bed with one of seven different speeds, ranging from 0.05 to 1.

The main properties of the results presented in Fig. 2 are as follows. As expected, slower intruders create shallow craters; specifically, the penetration depth is less than the intruder's own diameter. By contrast, intruders of higher speeds are entirely submerged in the granular bed. For the larger impact velocities we find an overshoot in the penetration depth, that is, the intruder rebounds toward the surface of granular layer, as also observed experimentally [8,21]. The "stopping time"

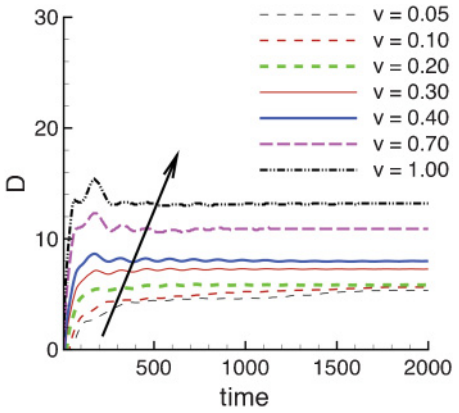

FIG. 2. (Color online) Penetration depth of $D_i = 10$ intruder impacting with different speed. Here we use $r = 0.2$, $k_n = 4 \times 10^3$, $k_t = 0.0$, $e_n = 0.5$, $\mu = 0.5$. Material properties of the intruder are the same as of the granular particles. The arrow shows the direction of increasing impact speed.

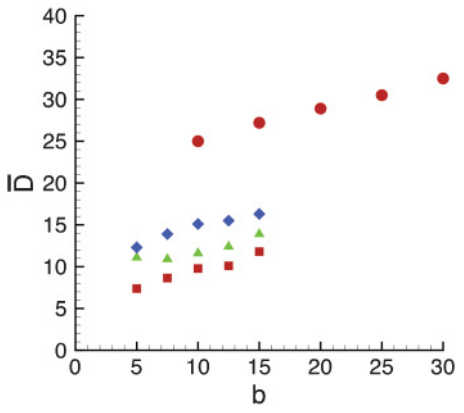

FIG. 3. (Color online) Total (long time) penetration depth $\bar{D}$ for intruders characterized by different elliptical ogives and different sizes; we show the results for (i) $a = 5$ and $v = 0.1$ (red squares), $v = 0.4$ (green triangles), $v = 0.7$ (blue diamonds), and for (ii) $a = 10$, $v = 0.7$ (red circles). The domain size was increased in (ii) to $H = 100$, $W = 100$. The other parameters are as in Fig. 2.

at which the intruder essentially stops is somewhat ambiguous for smaller impact velocities, for which there is no overshoot, and this time might be considered to be either approximately constant, as in [3], or a decreasing function of the impact velocity, as in [7].

The origin of the small oscillations seen in plots of the intruder depth versus time for longer times in Fig. 2 will be discussed later. Here we proceed to analyze the influence of the properties of the intruder and of the granular system itself on the penetration depth.

A. Intruder properties

Effect of shape: Realistic intruders are often not circular, and therefore it is relevant to explore the influence of the intruder shape on the interaction with granular matter. This issue was considered experimentally [22], and it was found that as expected, more pointed objects penetrated deeper, although only in the case of shallow penetration. To be specific, we consider here a particular shape, an elliptic ogive (an ellipse in 2D), and examine how the aspect ratio affects the penetration depth. To avoid complications with ogival intruders "falling" sideways as may happen particularly for impacts with low speeds, we prevent them from rotating simply by switching off the rotations of the intruder throughout the simulation. This is done for ogival intruders only and we have verified that for high speed impact (where the intruders do not fall sideways with or without rotations), there is no influence of exclusion of rotations on the final penetration depth.

As explained in Sec. II, we simulate elliptic intruders by preparing a "composite" intruder made up from rigidly attached particles. To isolate the effect of the intruder's shape, we fix the intruder masses to that of a disk with $D_i = 2a$ by changing the intruders' density. Figure 3 show the final (long time) penetration depth of the intruders characterized by different a, b, and impact velocities. We find that for the intruder sizes and aspect ratios considered here, the final penetration depth increases approximately linearly with the aspect ratio b.

Effect of composition and stiffness: The equations of motion determining the intruder's dynamics are also influenced by the moment of inertia. To consider the influence of this quantity, we consider hollow intruders, consisting of only a shell of thickness d. In order to ensure that the composite intruders behave identically to a single particle, we model solid intruders using both approaches. All three configurations (single-particle solid, composite solid, and composite hollow) yield essentially identical results, showing that (i) modeling of an intruder either as a composite or as a single particle produces indistinguishable results, and (ii) the influence of moment of inertia of an intruder, at least with the present choice of parameters, and for an intruder which is forced to remain straight as discussed before, is minimal. We have also considered briefly the influence of the projectile's stiffness on penetration, and simulated infinitely stiff intruders (limit of infinite spring constant k_n in our force model) interacting with soft granular particles. We find that the penetration depth for these stiff intruders is only slightly smaller compared to the finite-k_n ones. This result suggests that direct interaction of an intruder with granular particles plays only a minor role in determining final presentation depth, while particle-particle interactions are more relevant. This interaction is discussed next.

B. System properties

Effect of particle stiffness and the coefficient of restitution: Particle stiffness, modeled by the spring constant k_n, defines the collisional time scale in the problem $\tau_c \propto 1/\sqrt{k_n}$. Conceivably, one might expect that as k_n varies at constant (nondimensional) impact speed, the results would not change. That is, dynamics expressed in units of τ_c might be independent of dimensional properties such as k_n. However, this invariance is broken by the presence of gravity. While the role of gravity is explicitly considered later, we can already see its influence on the dynamics in the results of Fig. 4. This figure shows that as k_n (of both granular particles and intruder) increases at fixed dimensionless impact speed, the impact depth becomes

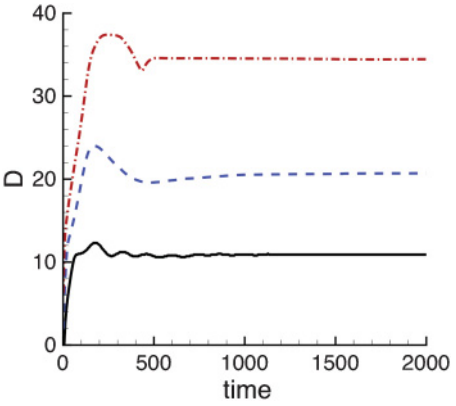

FIG. 4. (Color online) Penetration depth of an intruder in systems with varying stiffness (both intruder's and granular particles' stiffness is modified consistently). Here the force constant is given the following values: $k_n = 4.0 \times 10^5$ (red dash-dotted line), $k_n = 4.0 \times 10^4$ (blue dashed line), $k_n = 4.0 \times 10^3$ (black solid line). The impact speed is $v = 0.7$. The fixed value of τ_c used for nondimensionalization of all results is obtained using $k_n = 4.0 \times 10^3$. The other parameters are as in Fig. 2.

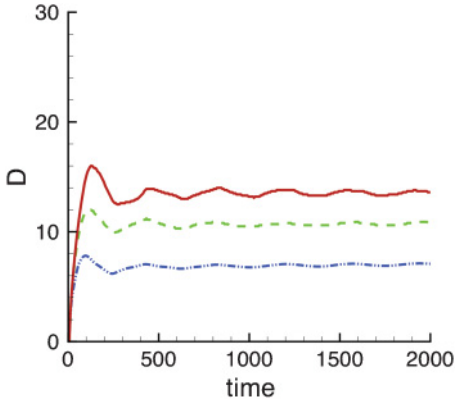

FIG. 5. (Color online) Penetration depth of an intruder in systems with varying coefficient of restitution, $e_n = 0.9, 0.5, 0.1$ shown by red (solid), dashed (green), and blue (dash-dotted) lines, respectively. Here $v = 0.7$, the system size is $W = 200$, $L = 200$; the other parameters are as in Fig. 2.

significantly larger. This result can be understood by realizing that the energy of impact is much larger in the case of larger k_n since impact velocity (in physical units) scales as $\sqrt{k_n}$. Note that larger stiffness is one of the reasons for significantly larger penetration depths in recent simulations [13], where stiffer particles were considered. An additional effect, the change of volume fraction due to modified interactions between the particles is weak, as noted in Sec. II. We have also considered impacts where the impact velocity is kept fixed (in physical units), and the stiffness changed. In this case we find at least for the parameters considered, the influence of particle (and intruder) stiffness on the penetration depth is minimal. The only visible influence of stiffness is modification of the initial overshoot which is less pronounced for stiffer particles. This effect can be explained by stronger resistance of stiffer particles during the initial stage of (relatively) high-speed impact. For the impacts characterized by low speed, we do not see any influence of stiffness.

Figure 5 shows the influence of elasticity of the granular particles, measured by the coefficient of restitution e_n. A large coefficient of restitution leads to a significantly deeper penetration, as would be expected since the energy loss is reduced relative to a lower restitution coefficient. Interestingly, while a decrease of e_n reduces the depth of penetration, it does not remove the overshoot of the $D(t)$ curve. We will see below that a different behavior results when the frictional properties of granular particles are modified. Later in this section we will also discuss the influence of e_n on the long-time oscillations of the projectile depth $D(t)$; for the purpose of this later discussion we use a larger domain size for the simulations shown in Fig. 5.

Effect of friction: The influence of friction between the granular particles on the penetration depth in particular, and on the response of the granular material to an intruder in general is not immediately obvious. For example, in considering the response of a system to a point force, it has been found that friction plays a role in determining how forces and stresses propagate through the system [20]. Of course, a response to an intruder is expected to be more complicated since it leads to a large scale rearrangement of granular particles, which is not expected in a response to a localized (small) point force. Indeed, it has been suggested that friction is not necessarily crucial in understanding this response [13]. Here we illustrate the influence of friction on the penetration depth for a particular system. We discuss more generally the manner in which friction influences the dynamics of an intruder in the Appendix, and the corresponding behavior of the granular material of different frictional properties in Sec. IV.

To illustrate the influence of friction we consider two effects: first, the effect of the friction model, and second of Coulomb threshold. Figure 6 shows the corresponding results. We find that having a model with static friction leads to a significantly smaller penetration depth (blue dash-dotted curve in Fig. 6) than a model without static friction, particularly for a large Coulomb threshold. For a smaller Coulomb threshold, the influence of static friction is weaker, and the response

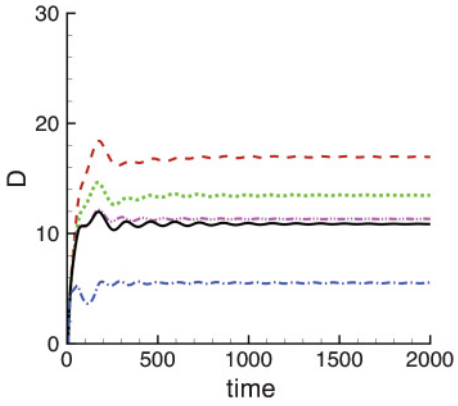

FIG. 6. (Color online) Penetration depth for different friction models and Coulomb thresholds; here we show the results as follows (top to bottom): $\mu = 0$ (red dashed line); $\mu = 0.1, k_t = 0.0$ (green dotted line); $\mu = 0.1, k_t = 0.8$ (pink dash-dot-dotted line), $\mu = 0.5$, $k_t = 0.0$ (black solid line); $\mu = 0.5, k_t = 0.8$ (blue dash-dotted line). Here $v = 0.7$, the other parameters are as in Fig. 2.

of the system in that case turns out to be similar to the one obtained using kinetic friction only (compare green dotted and pink dash-dot-dotted curves in Fig. 6). Furthermore, an "overshoot" in the intruder depth may be removed in the case of (strong) static friction. This is one significant difference between the influence of friction and inelasticity on the intruder's dynamics: in the case of increased inelasticity (smaller coefficient of restitution) we still find an overshoot, see Fig. 5.

Effect of polydispersity: One of the focal points of this work is the influence of granular microstructure on impact. Microstructure is strongly influenced by the polydispersity and related structural ordering of granular particles. To analyze the influence of these parameters, we have carried out simulations where we have varied the parameter r determining polydispersity between 0.0 and 0.4. We have also carried out simulations using a perfect hexagonal lattice of particles as the initial configuration. We typically find that the results for a system with $r = 0.0$, prepared as described in Sec. II, are similar to the ones obtained using a hexagonal lattice. This is not surprising since monodisperse particles tend to crystallize, as confirmed by considering the pair correlation function, which shows only small differences between monodisperse "random" and hexagonal lattices. (These results are not shown here for brevity.) Therefore we show the results obtained using a hexagonal lattice in place of an $r = 0.0$ system prepared using our usual protocol.

Figure 7 shows the intruder depth as a function of time for an impact on a hexagonal lattice. We immediately note very different properties of the $D(t)$ curves compared to an impact on a polydisperse system, see Fig. 2. For the impact velocities considered here, the intruder very quickly reaches a depth at which its velocity reverses, and then the intruder actually rebounds *outside* of the granular layer, falls again under gravity, and then settles at the final depth. This final depth does not depend in any obvious manner on the impact velocity, presumably because the impact is not strong enough to initially penetrate through the lattice structure of the material, and by the time of the secondary impact (after rebound), the information about the initial velocity has been lost. The initial velocity essentially influences only the initial depth which

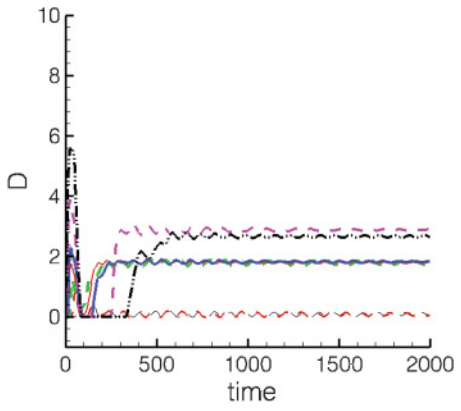

FIG. 7. (Color online) Penetration depth for an impact on a hexagonal lattice; here $r = 0.0$ and the other parameters and line patterns are as in Fig. 2. Note the different range on the vertical axis compared to the one typically used.

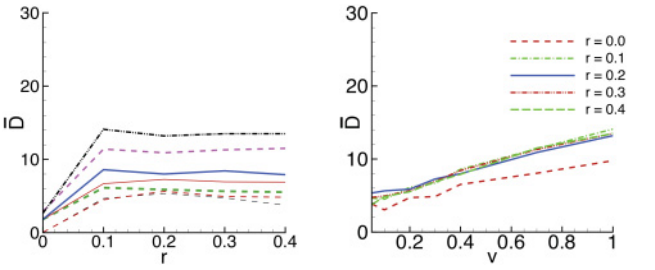

(a)penetration depth as a function of r for different v's. (b)penetration depth as a function of v for different r's.

FIG. 8. (Color online) Final (long time) penetration depth for the systems characterized by different polydispersities r; the other parameters are as in Fig. 2.

the intruder reaches (before rebound), and the length of the interval after impact which the intruder spends outside of the granular layer (this interval being longer for larger impact velocities). Finally, by comparing the final penetration depth between an impact on a hexagonal lattice, shown in Fig. 7, and on a disordered granular system, such as the one shown in Fig. 2, we note that the final penetration depth in the former case is much smaller. We will discuss the reasons for this difference later in Sec. IV.

Figure 8 shows in more detail how the final penetration depth depends on the polydispersity. To help interpretation of the results we show both the final depth as a function of r for fixed v [Fig. 8(a)] and the final depth as a function of v for fixed r [Fig. 8(b)]. Clearly the penetration is deeper in polydisperse systems compared to the hexagonal one for all considered impact velocities. However, we find that the degree of polydispersity has no significant effect on the penetration depth as long as the system is not monodisperse and ordered.

Figure 8(b) shows that the penetration depth depends approximately linearly on the impact speed of the intruder for larger velocities and deeper penetration. This observation agrees with results reported earlier [3,4,8], where it was found that the penetration depth increases linearly with the impact speed for a range of impact depths that are comparable or larger than the intruder size. For smaller impact velocities, we find deviations from the linear scaling, again consistent with the literature [2,5,6]. We discuss this scaling in some more detail in the Appendix.

Effect of gravity: We discuss here in more detail the influence of the acceleration of gravity on the penetration depth. As mentioned earlier, the value of the gravitational acceleration is expected to play a role since it influences the mobility of the particles following impact. Gravitational compaction itself is found to play just a minor role, as discussed in Sec. II. For brevity we consider the effect of gravity only for the system characterized by $r = 0.2$, $k_t = 0$. Here, as the initial configuration, we consider a system prepared under Earth's gravity and then left to relax until the total kinetic energy of the particles falls below a specified threshold ($10^{-10} mgd_{\mathrm{av}}$). Figure 9 compares the results for Earth's gravity with data for several other planets and satellites, specifically, Pluto, Moon, Mars, and Jupiter. We find significantly deeper penetration for smaller gravitational accelerations. At least for the parameters considered, we do not find robust scaling of

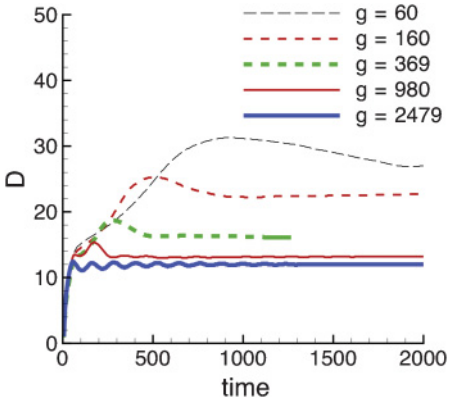

FIG. 9. (Color online) Influence of gravitational acceleration on impact; here $v = 1.0$ and the other parameters are as in Fig. 2. We chose g (given in cm/s^2), appropriate to various objects in the solar system: Pluto, Moon, Mars, Earth, and Jupiter.

$\bar{D}$ with g. An expanded discussion of possible scaling with g in other parameter regimes can be found in [7,8,10,13] and the references therein. Figure 9 also shows that the maximum penetration depth is reached at much later times as gravity is decreased, as expected from the discussion in [8,13] and in the Appendix.

Figure 10 shows the response to impact of granular particles under different gravity. Here the particles are colored according to the average normal force experienced (recall that the force is given in nondimensional units defined using Earth's gravity). We see significantly increased mobility of the particles after impact for smaller g, confirming the intuitive argument presented above. Note that we modify only the gravitational force on the particles and not their stiffness,

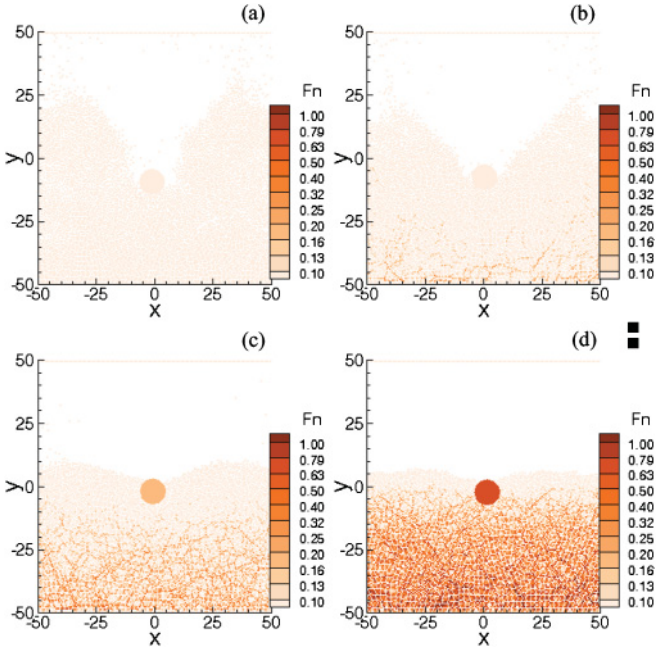

FIG. 10. (Color online) Snapshots of a granular system after impact under the four larger gravities considered here ($g = 160, 369,$ 980, and 2479 cm/s^2) from Fig. 9 at $t \approx 300$. Gravity is monotonously increasing from (a) to (d).

which remains the same. We also note that the change of impact speed due to modified gravity is minor, only a fraction of a percent.

Effect of system size and initial configuration: System size has been recognized in previous work as one of the factors which may influence the results [7,12,13,23–25]. To explore this effect we have carried out additional simulations where the system size was varied. Since modifying the system size also requires changing the configurations of the particles, we also consider the issue of reproducibility here, that is, we consider the variations between realizations for the same macroscopic parameters. Changing the initial particle configuration may lead to different dynamics, and the different realizations give us a measure of statistical fluctuations on macroscopic results such as the penetration depth.

Figure 11 shows results for six different system sizes, corresponding to different initial widths of the granular layer W and the domain size in the horizontal direction L. First we note that despite different visual appearances of the detailed trajectories, the final penetration depth (the value reached for long times) varies only very little (less than a particle diameter)

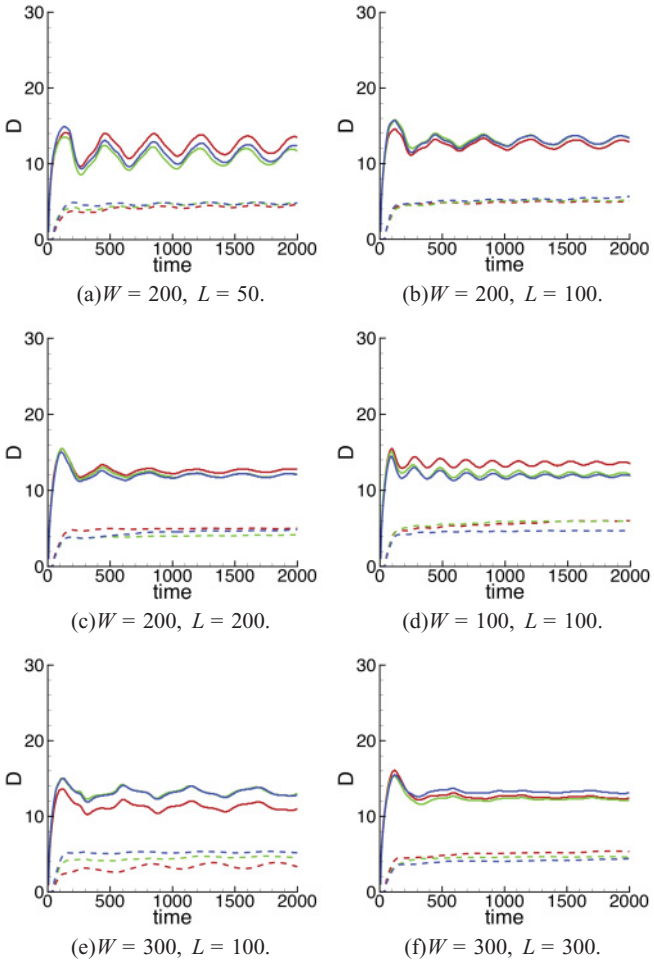

FIG. 11. (Color online) Influence of the initial system width W and length L on the penetration depth as a function of time. The solid and dashed lines show three realizations of impacts with the speed $v = 1.0/0.1$, respectively. The other parameters are as in Fig. 2.

between systems of different sizes. This variation is smaller than that due to different initial conditions, and therefore we conclude that for the systems considered here the system size is sufficiently large that there is no significant influence on the final penetration depth. This observation agrees with the experiment results found in [24] and [26]. We note in passing that the presence of the overshoot in $D(t)$ is not influenced by the system size, as also found in a recent experimental work [8].

Next, we comment on the oscillations of the penetration depth that are clearly visible in Fig. 11. Perhaps contrary to an intuitive expectation, these oscillations *do not* decrease for the largest systems considered here; on the contrary, they increase in amplitude. Below we first discuss the origin of these oscillations, and then their dependence on the system size.

Recall that the penetration depth is defined with respect to the position of the top surface of the granular system at initial time $t = 0$. During an impact, the kinetic energy of the intruder is mostly transferred into elastic energy that propagates through the system in the form of (damped) elastic waves (see, e.g., [27]). (Note that some of the energy goes into friction; this issue is discussed briefly in the Conclusions.) These elastic waves interact with the system boundaries, and in the case of the bottom boundary they partially reflect and lead to an expansion of the whole granular bed. We have confirmed this by comparing the period of oscillations visible in Fig. 11 with the time it takes for the elastic waves to cross the system twice. For example, note that for shallower systems the period of the oscillations is shorter, as expected based on the above argument. It is important to note that for the present choice of parameters these elastic waves do not influence in any significant manner the motion of the intruder *relative* to the granular particles surrounding it: they essentially lead to global oscillations of the system. To confirm this statement, Fig. 12 shows the depth of the intruder with respect to the *time-dependent* position of the interface, calculated at the same time as the intruder's position. The long-time oscillation are not visible anymore. A different regime, with intruders comparable in size to the granular particles, and therefore more susceptible to the pressure

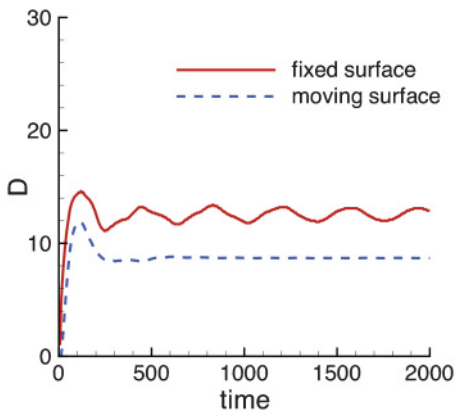

FIG. 12. (Color online) Penetration depth for a system characterized by $L = 100$ and $W = 200$; the impact speed is $v = 0.7$; the other parameters are as in Fig. 2.

due to the propagating elastic waves, has been discussed recently [12].

The next question is the influence of the system size in the horizontal direction L on the oscillations. Again, for the sizes considered, there is no influence on the final penetration depth. More narrow systems (with smaller L), however, lead to increased amplitude of the oscillations. This is a consequence of our periodic boundary conditions imposed at the right and left boundaries: the waves propagating right and left from the impact point "re-appear" from the other side of the domain and increase the oscillatory behavior. In the case of large systems these waves lead to nonsinusoidal oscillations, as can be seen in Fig. 11(f).

The final question is why the oscillations do not diminish with the system depth W. The answer to this question has to do with the properties of the elastic waves propagating through the system. It is known that propagation is enhanced in systems characterized by stronger compression, or, correspondingly to some degree, larger volume fractions, as discussed recently [27]. In larger systems there is stronger gravitational compaction in the deeper layers, leading to stronger wave propagation and rebound, and correspondingly, to more visible oscillations. This conjecture is supported by the results for different gravity (Fig. 9), where we observe that in the systems under smaller gravity the oscillations are weaker as well. We note that for significantly larger systems compared to the ones considered here, one expects that damping and/or friction would be strong enough to reduce or eliminate the influence of elastic waves. As one might expect, stronger damping significantly reduces the amplitude of the oscillations, as shown for the systems considered here in Fig. 5.

We note that to our knowledge these oscillations have not been yet observed experimentally. Their eventual observation may provide a new insight regarding response of a granular system to an impact, and improve our understanding of the influence of impact and resulting acoustic waves on granular dynamics.

IV. MICROSTRUCTURE EVOLUTION, FORCE NETWORKS, AND GRANULAR DYNAMICS DURING IMPACT

In this section we discuss the internal response of the granular system to impact, and the role which microstructure plays in determining the macroscopic results, such as penetration depth. We concentrate in particular on the role of polydispersity, ordering, and friction in determining the granular response. We consider two separate sets of measures to quantify the response: (i) the geometric and topological properties of the force field evolving in a granular system during impact, and (ii) the dynamics of the granular particles quantified by measuring affine (conforming) and nonaffine (nonconforming) components of granular motion.

A. Properties of the force field

Figures 13–16 show snapshots of the normal and tangential forces which granular particles experience due to impact on a polydisperse system at four different times. Animations of the impact are available as Supplementary Materials [28].

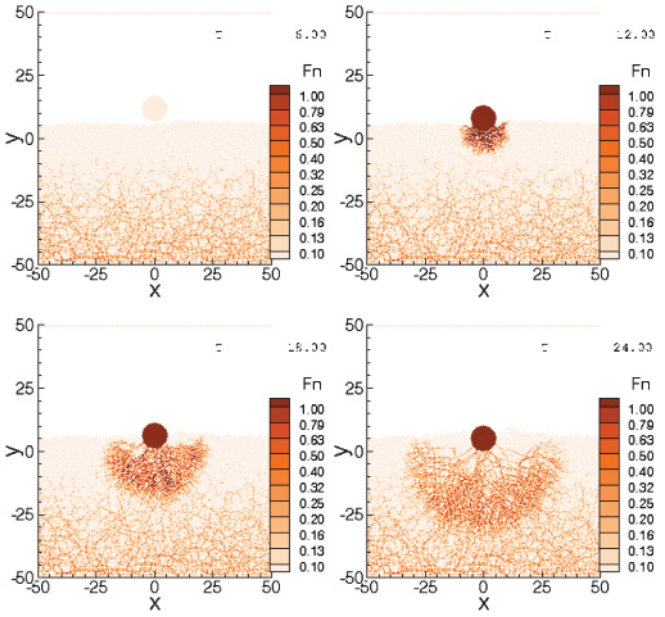

FIG. 13. (Color online) Normal force experienced by the granular particles at four different times. Here $v = 0.7$, and the other parameters are as in Fig. 2 (kinetic friction). Animations are available [28].

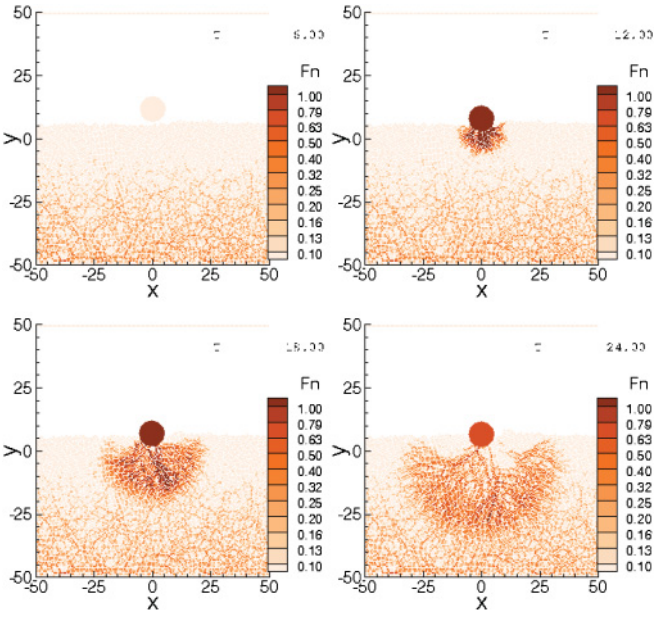

FIG. 15. (Color online) Normal force experienced by the granular particles at four different times for $k_t = 0.8$; the other parameters are as in Fig. 13 (static friction). Animations are available [28].

Before the impact itself (part a) we see the force chains due to gravitational compaction, already discussed earlier. During the impact we observe approximate isotropic expansion of the area in which particles experience large normal force. Properties of this large-force area are discussed next.

One issue of interest is the influence of intergranular friction on the force field. By comparing Figs. 13 and 15 we find no significant differences, suggesting that the friction model is not crucial in determining the properties of the normal force field between the granular particles. On the other hand, Figs. 14 and 16 suggest that tangential forces depend strongly on the friction model. Recalling now that the penetration depth is much smaller for the particles modeled by static friction and large Coulomb threshold (see Fig. 6) we conclude that at least for the systems considered, tangential forces are the ones which play a significant role in determining the dynamics and final penetration depth of an intruder. The influence of friction on

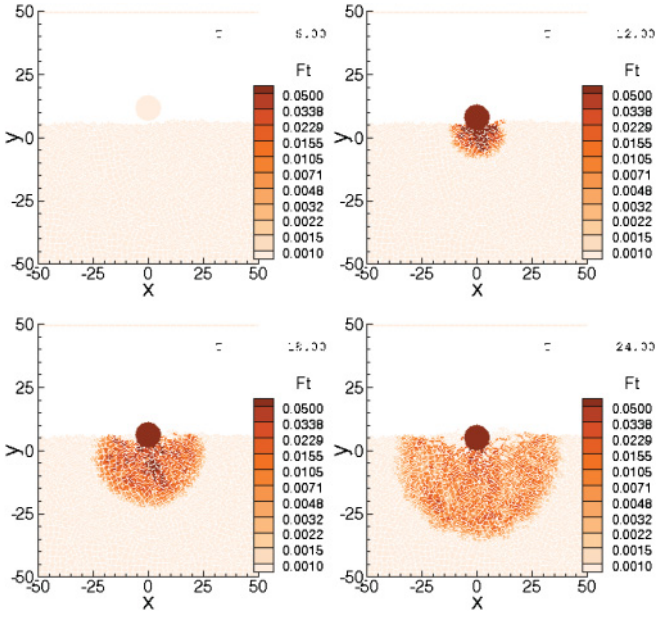

FIG. 14. (Color online) Tangential force experienced by the granular particles at four different times for the same parameters as in Fig. 13 (kinetic friction). Note different range of the force magnitudes shown compared to Fig. 13. Animations are available [28].

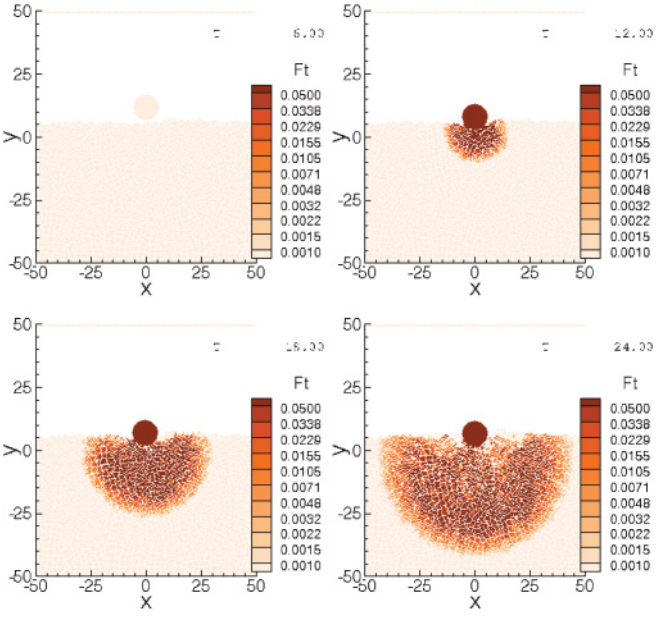

FIG. 16. (Color online) Tangential force experienced by the granular particles at four different times for the same parameters as in Fig. 15 (static friction). Animations are available [28].

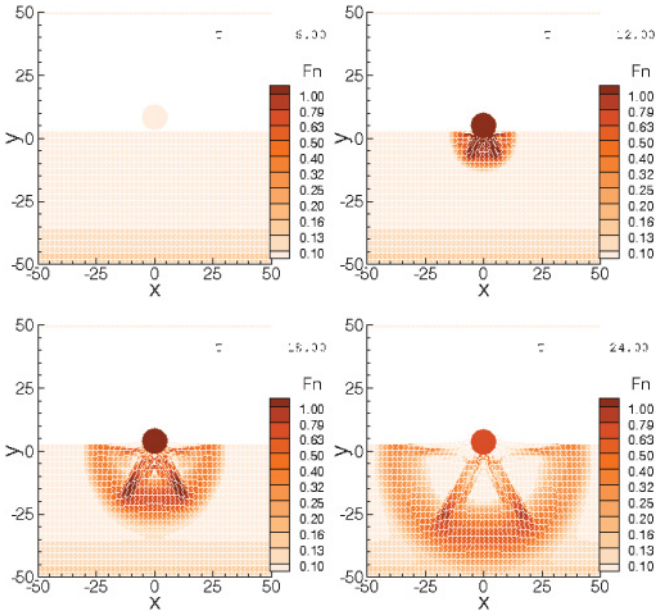

FIG. 17. (Color online) Normal force experienced by the granular particles at four different times during impact on a hexagonally ordered system. Here $r = 0.0$ and the other parameters are as in Fig. 13 (kinetic friction). Animations are available [28].

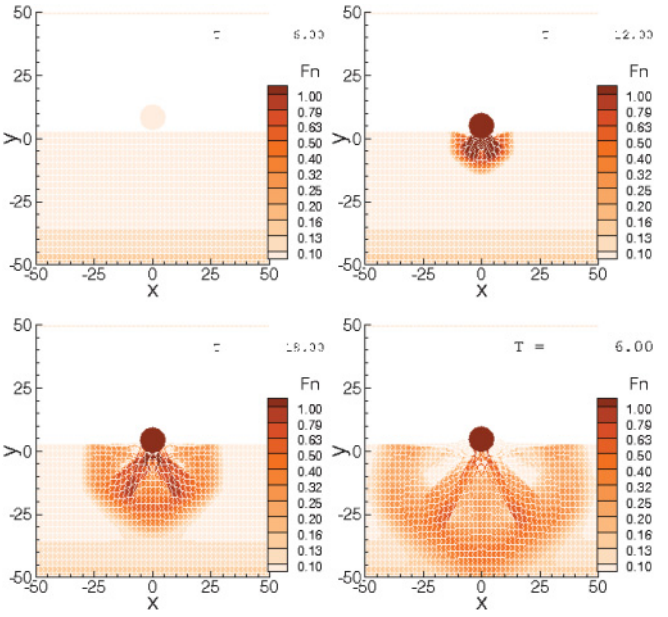

FIG. 19. (Color online) Normal force experienced by the granular particles at four different times for $k_t = 0.8$; the other parameters are as in Fig. 17 (static friction). Animations are available [28].

the force networks is even more obvious in the impact on a hexagonally ordered system, which we discuss next.

Figures 17 to 20 show the structure of the normal and tangential force field during impact on an ordered, hexagonal system. We find that the forces propagate in a very different way, compared to what we find for an impact on a random, polydisperse system: in the case of the ordered packing, we see predominant propagation in the lattice directions, combined with a (weaker) uniform, isotropic front. Therefore we conclude that geometric microstructure plays a significant role in determining the force field in a granular system. We note that any degree of polydispersity and related disorder leads to a transition from ray-like propagation, shown in Figs. 17 and 19, to isotropic propagation, seen in Figs. 13 and 15. We have confirmed this by carrying out corresponding simulations with smaller r (not shown here for brevity). Since we observe larger magnitudes of the forces in the ordered system, we expect that these larger forces manifest themselves as larger forces on the intruder itself, and therefore lead to more shallow

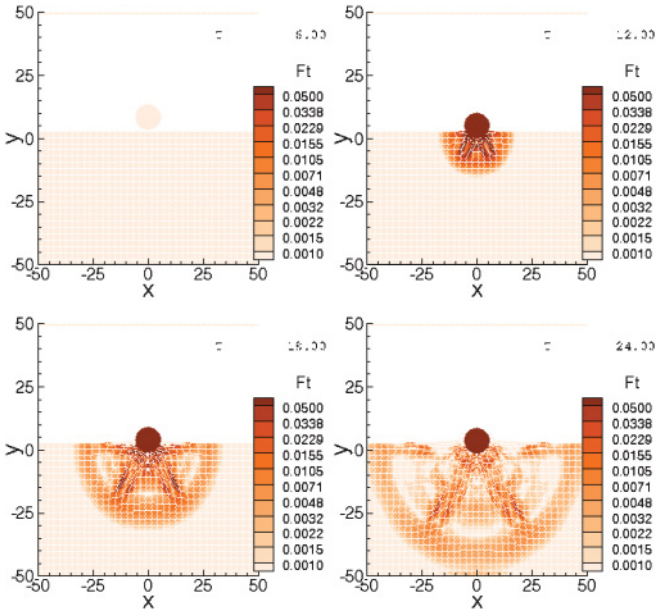

FIG. 18. (Color online) Tangential force experienced by the granular particles at four different times for the same system as in Fig. 17 (kinetic friction). Animations are available [28].

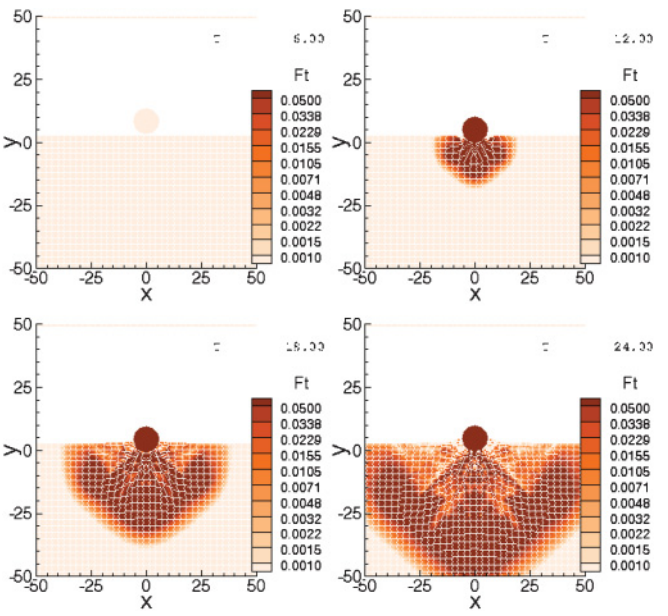

FIG. 20. (Color online) Tangential force experienced by the granular particles at four different times for the same system as in Fig. 19 (static friction). Animations are available [28].

penetration (see Fig. 8). These findings regarding the influence of polydispersity are consistent with other recent work, where the response of three-dimensional frictionless systems to a localized perturbation was considered [29,30].

Next we discuss the influence of friction on force propagation in an ordered system. Regarding normal forces, by comparing Figs. 17 and 19, we again see no significant differences on the temporal and spatial scales considered. However, one can still observe the effect of friction on some features of force propagation, which have been discussed recently from the point of view of elastic versus hyperbolic force propagation [20,31]. Static friction is expected to lead to a more elastic-like response, that is, the force (or pressure) on granular particles is expected to reach a maximum value directly below the source, while kinetic or no friction is expected to lead to a more a hyperbolic-like response with a pressure dip below the source. By comparing the results in Figs. 17 and 19 at $t = 24$, one can observe a variation of this effect with the significantly more pronounced force dip below the source for kinetic friction case. We note that having an ordered structure is important to observe this effect; polydispersity and associated disorder have masked it in Figs. 13 and 15, which show the normal force for a polydisperse system.

As for the disordered system discussed above, the influence of friction model is much more significant for tangential forces than for normal forces. Figures 18 and 20 illustrate this effect. In addition to observing significantly larger tangential forces when static friction is included, we again find more hyperbolic-like force propagation in the case of kinetic friction, and a more uniform, elastic-like response when static friction is present.

Figure 21 shows F, the total force on the intruder in the y direction, for different friction models and polydispersities and ordering. We see that this force is very large immediately after impact, and then decreases significantly on a very short time scale. The second, much smaller peak in the force visible in some of the results is due to reflected elastic waves as discussed before. The influence of these waves on the intruder dynamics is minor. While we note larger force for impact on polydisperse particles with a static friction model [blue dash-dotted line in Fig. 21(a)], perhaps the most important observation regarding

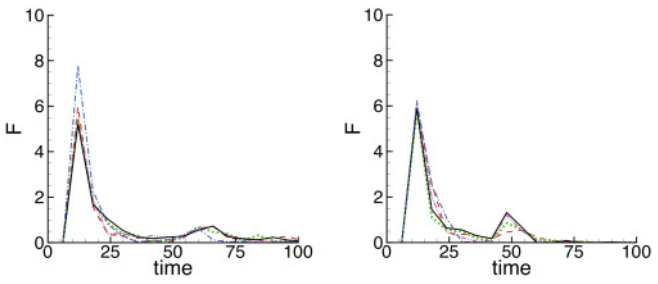

(a) polydisperse, $r = 0.2$. (b) hexagonal, $r = 0.0$.

FIG. 21. (Color online) The total force on the intruder as a function of time for the following systems [depth vs time for the systems in part (a) is available in Fig. 6]: $\mu = 0$ (red dashed line); $\mu = 0.1, k_t = 0.0$ (green dotted line); $\mu = 0.1, k_t = 0.8$ (pink dash-dot-dotted line), $\mu = 0.5, k_t = 0.0$ (solid black line); $\mu = 0.5, k_t = 0.8$ (blue dash-dotted line). Here $v = 0.7$; the other parameters are as in Fig. 2.

the results shown in this figure is how similar they are for the different systems considered here, suggesting that it may be difficult to extract the main features about the intruder's dynamics based on this information alone. Recall that the penetration depths differ significantly between the different friction models and different polydispersities.

The force fields, in particular in disordered systems, may have very complicated structures. Therefore it is difficult to extract their generic properties, and to reach, for example, an answer to the question of global changes of the force field due to an impact. For this reason, we consider topological properties of the force network, by computing its connectivity. One measure of the connectivity can be formulated in terms of Betti numbers, which are global topological measures specifying the properties of a network [32]. In particular, the zeroth Betti number, B0, measures the number of connected components, and the first Betti number, B1, measures the number of holes inside a network. Clearly these quantities depend on the force threshold chosen. For example, if one chooses zero threshold (considering all the particles), B0 will provide an information about the packing of the material. As the force threshold is increased, the number of particles experiencing a force larger than a given threshold decreases, and consequently the topology of the network changes. The computations are carried out using the publicly available software package CHOMP [33]. These computations involve thresholding a particular force level and producing a binary image (black less than or equal to the threshold and white above the threshold), and then computing Betti numbers, hence measuring the connectivity of the resulting images. Here we will concentrate only on B0, with the main goal of quantifying the differences between the force networks developing during impact for different friction models, and for different polydispersities. We note that here we explore connectivity on the particle scale; an alternative approach where connectivity is considered on the level of individual contacts is possible as well [34]. Future work should address the differences, if any, resulting from these two different approaches to computing connectivity. For brevity, here we concentrate only on the force fields in polydisperse systems.

Figure 22 shows B0 for the impact on a polydisperse system with (a) kinetic and (b) static friction. The snapshots of the corresponding force field for part (a) can be seen in Fig. 13. We see that for very small and for very large forces, the B0 are very small since for very small forces all particles are found to form a cluster (due to being in contact with each other), while the number of particles experiencing very large forces is small, so that there are no components (clusters) to be seen. The main difference between the the two parts of the figures is a larger number of components (clusters) for the system where static friction is included. Recalling more shallow penetration for the system where static friction is included, we conjecture that there is a correlation between larger number of components (clusters) and corresponding resistance to an impact. To our knowledge, this influence of static friction on the structure of force network has not been discussed previously in the literature.

Figure 23 shows the tangential forces for the same system as in Fig. 22. The information which can be obtained from this figure is consistent with the insight which we reached by

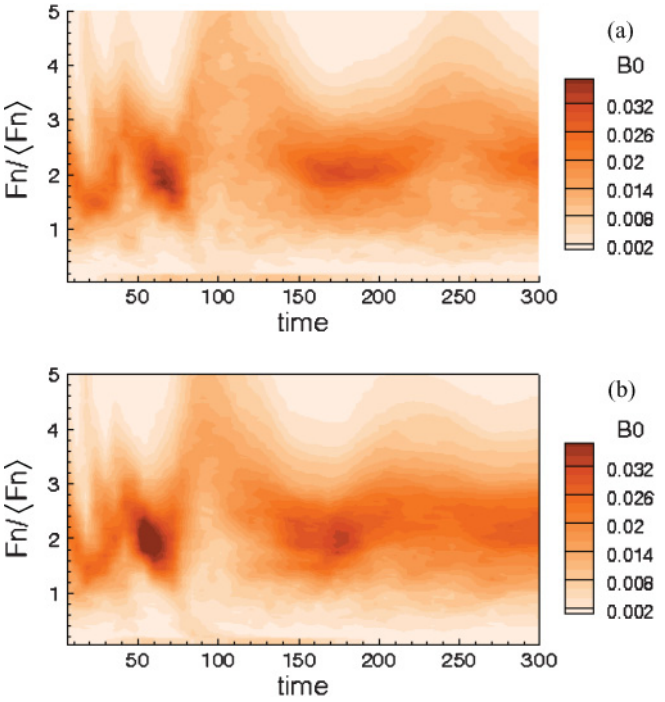

FIG. 22. (Color online) Zeroth Betti number B0 for the normal force during impacts on polydisperse, $r = 0.2$, systems with $v = 0.7$ and (a) kinetic friction; (b) static friction; the other parameters are as in Fig. 2. In this and the following figure, B0 are normalized by the number of particles, and the forces by the average (normal) force on all particles. Note that the peaks in the B0 for $F_n/\langle F_n\rangle \approx 2$ (perhaps more visible in the following figure) are due to the elastic waves propagating through the system.

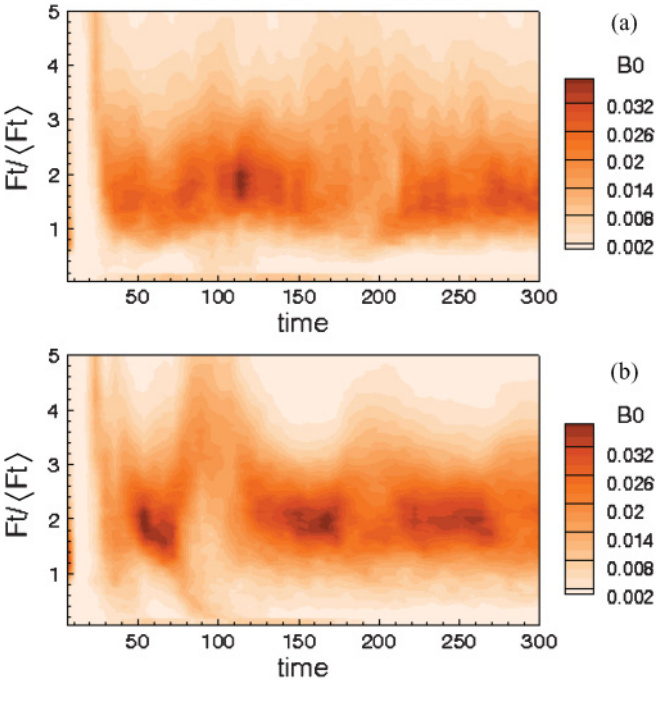

FIG. 23. (Color online) Zeroth Betti number B0 for the tangential force during impacts on the systems as in Fig. 22.

considering the normal forces: larger number of components (clusters) for the systems where static friction is present.

We conclude by summarizing our current results regarding properties of the force field during an impact. For disordered, polydisperse system, we find the following:

(1) The main influence of static friction on the force field is a significant increase of tangential forces.

(2) Both normal and tangential forces show increased ramification (in the sense of increased number of components (clusters)) in the presence of static friction.

For monodisperse, ordered systems, we find

(1) As for polydisperse systems, there is only a minor influence of friction on the normal forces, while tangential forces are increased strongly when static friction is included. In addition, the total force on an intruder is similar for monodisperse ordered and polydisperse disordered systems, suggesting that it may be difficult to extract information about the intruder's dynamics based on the information about the total force on the intruder alone.

(2) The normal force field is highly uniform; however, the tangential force field is much more structured, suggesting that a significant amount of disorder of the tangential interactions between the particles is introduced during an impact.

We note that the current results concentrate only on the global, large scale features. More work is needed to analyze the detailed, local, properties of the force fields, including their temporal evolution.

B. Properties of the displacement field

Next, we consider dynamics of the granular particles due to impact. For this purpose we compute the displacement field using the approach from [35], outlined briefly in what follows. The displacement field shows how granular particles respond to an impact, and will allow us to correlate granular response and dynamics of the impactor. The approach of Falk and Langer [35] allows one to compute both affine (conforming) and nonaffine (nonconforming) parts of the displacement field. The affine part, providing information about the dominant component of granular dynamics, is of particular interest for the present problem since the basic locally coarse-grained solution is not known. The nonaffine part can be associated with plastic deformation of granular system due to impact, leading to irreversible changes of the granular structure

The affine and nonaffine components are computed as follows. For each particle, a circle of radius R centered at the particle is defined, and all the particles in this circle are considered to be its neighbors. We choose the size of this circle to be $R = 2.5d$. Let us denote by $\mathbf{r}_0(t)$ the position of this central particle and by $\mathbf{r}_m(t), m = 1, \ldots, n$ the positions of its neighboring particles, respectively. Then, the displacement of one neighboring particle relative to the central one is given by $\mathbf{r}_n(t) - \mathbf{r}_0(t)$ at time t. Assuming only conforming (affine) deformations are present, we denote them by

$$\mathbf{r}(t + \delta t) = \mathbf{A}(t) \cdot \mathbf{r}(t),$$

where $\mathbf{A}(t)$ is a 2×2 matrix. Under the affine deformation, the displacement of the neighboring particle relative to the central one becomes

$$\mathbf{A}(t) \cdot \mathbf{r}_n(t) - \mathbf{A}(t) \cdot \mathbf{r}_0(t). \quad (3)$$

To measure the difference between an actual deformation and the affine part we define the quantity $\mathcal{D}^2$ as the mean-square difference between the actual displacement $\mathbf{r}_n(t) - \mathbf{r}_0(t)$ and the one defined by Eq. (3), that is,

$$\mathcal{D}^2 = \sum_{n=1}^{m} \|\mathbf{r}_n(t+\delta t) - \mathbf{r}_0(t+\delta t) - \{\mathbf{A}(t)\cdot[\mathbf{r}_n(t) - \mathbf{r}_0(t)]\}\|^2. \tag{4}$$

Then we find the minimum $\mathcal{D}^2_{\min}$ of $\mathcal{D}^2$ by minimizing $\mathcal{D}^2$ with respect to the four elements of $A(t)$, that is,

$$\mathbf{A}(t) = \begin{bmatrix} A_{11}(t) & A_{12}(t) \\ A_{21}(t) & A_{22}(t) \end{bmatrix}.$$

We obtain the expression for $\mathbf{A}(t)$ and the corresponding nonaffine component $\mathcal{D}^2_{\min}$. The magnitude of $\mathcal{D}^2_{\min}$ indicates the local nonaffine component of displacement in the vicinity of each particle. In addition, we can retrieve the affine component from $\mathbf{A}(t)$.

Figure 24 shows snapshots of the affine deformation for the polydisperse systems characterized by different friction models. We show the x and y components of the vector $\mathbf{A}_f = \mathbf{A}\cdot[\mathbf{r}(t) - \mathbf{r}(t-\delta t)]$. These figures reveal outward motion of the granular particles away from the point of impact [Figs. 24(a) and 24(b)], downward motion in the area below the impact, combined with the upward motion at the surface of the granular bed just next to the impact point. While the results for the two systems are fairly similar, we see increased mobility for the particles experiencing kinetic friction only, in particular for the y component of affine deformation.

Figure 25 shows $D^2_{\min}$, measuring the strength of the nonaffine component. This component of motion is more prominent for the case where only kinematic friction is present;

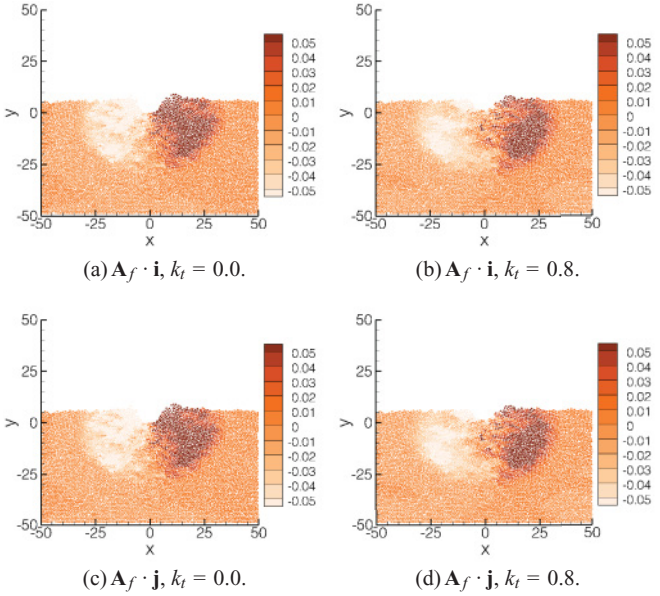

(a) $\mathbf{A}_f\cdot\mathbf{i}$, $k_t = 0.0$. (b) $\mathbf{A}_f\cdot\mathbf{i}$, $k_t = 0.8$.

(c) $\mathbf{A}_f\cdot\mathbf{j}$, $k_t = 0.0$. (d) $\mathbf{A}_f\cdot\mathbf{j}$, $k_t = 0.8$.

FIG. 24. (Color online) Affine deformation at $t = 24$ for impact on polydisperse systems modeled by different friction models: kinetic [(a) and (c)] and static [(b) and (d)]. Here $\mathbf{i}$ and $\mathbf{j}$ are the unit vectors in the x and y directions, and $v = 0.7$. The other parameters are as in Fig. 2.

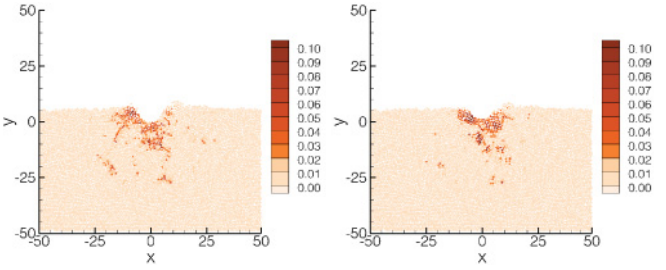

(a) $k_t = 0.0$. (b) $k_t = 0.8$.

FIG. 25. (Color online) $D^2_{\min}$ distribution at $t = 24$ for impact on polydisperse systems modeled by different friction models: kinetic (a) and static (b). The other parameters are as in Fig. 24.

however, the differences between the two cases are only moderate.

Precise information about affine and nonaffine components of granular dynamics for hexagonally ordered systems is also of interest. Figures 26 and 27 show corresponding results, again for the systems characterized by kinematic and static friction, for the hexagonally ordered systems. Here we also include the L_2 norm of the affine deformation since it provides useful additional insight. Figure 26 shows stronger affine deformation for the kinetic friction case, particularly visible

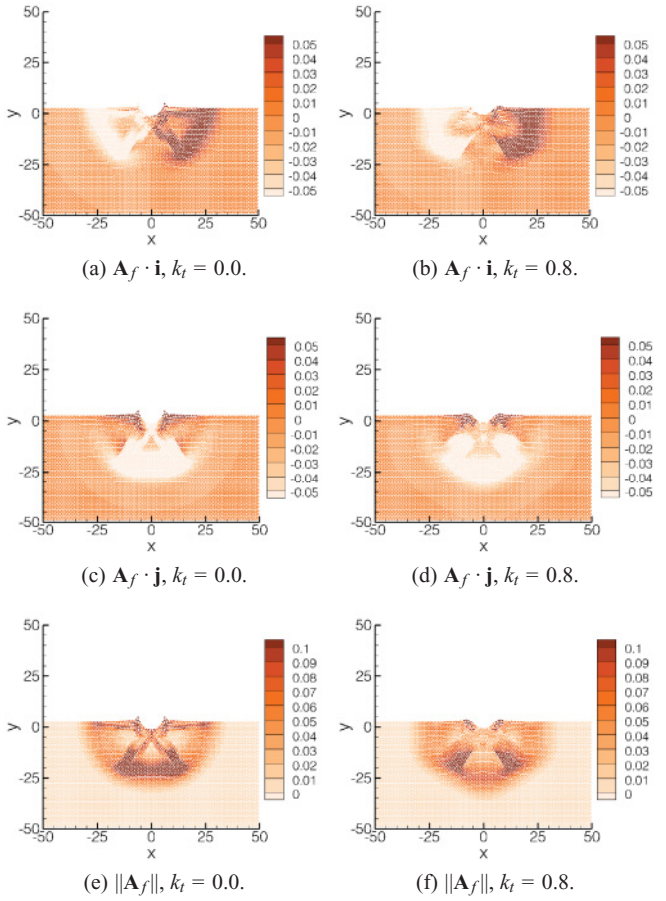

(a) $\mathbf{A}_f\cdot\mathbf{i}$, $k_t = 0.0$. (b) $\mathbf{A}_f\cdot\mathbf{i}$, $k_t = 0.8$.

(c) $\mathbf{A}_f\cdot\mathbf{j}$, $k_t = 0.0$. (d) $\mathbf{A}_f\cdot\mathbf{j}$, $k_t = 0.8$.

(e) $\|\mathbf{A}_f\|$, $k_t = 0.0$. (f) $\|\mathbf{A}_f\|$, $k_t = 0.8$.

FIG. 26. (Color online) Affine deformation at $t = 24$ for impact on monodisperse hexagonal systems modeled by different friction models: kinetic [(a) and (c)], and static [(b), (d), and (e)]. Here $v = 0.7$ and the other parameters are as in Fig. 2.

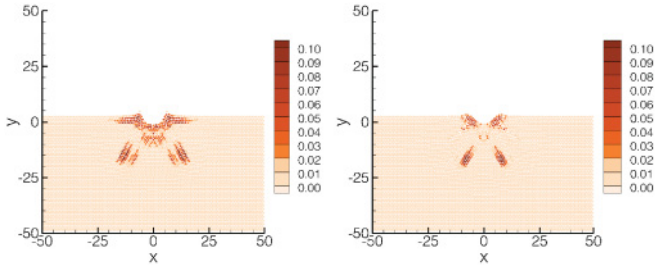

(a) $k_t = 0.0$. (b) $k_t = 0.8$.

FIG. 27. (Color online) $D^2_{\min}$ distribution at $t = 24$ for impact on polydisperse systems modeled by different friction models: kinetic (a) and static (b). The other parameters are as in Fig. 26.

when considering the norms [Figs. 26(e) and 26(f)]. Granular particles interacting only by kinetic friction clearly respond stronger to an impact. Consistently, Fig. 27 then shows that nonaffine component is also much more pronounced for the kinetic friction case, suggesting that static friction also reduces nonaffinity of particle motion.

V. CONCLUSIONS

In this work we analyze the response of a granular system to an impact, with particular emphasis on understanding the influence of granular microstructure on intruder dynamics. In particular, we present a precise descriptions of the force and displacement fields, which have not been discussed previously with this level of detail. The results show that the grain-scale properties play a crucial role in determining the dynamics of an intruder. The main findings are as follows:

(1) Force propagation in a granular system is strongly influenced by structural ordering. The total penetration depth is significantly smaller for impacts on ordered granular material.

(2) Frictional interactions and the resulting tangential forces between the particles play a major role in determining the final penetration depth, at least for the considered parameters. Both the type of frictional model used (static versus kinetic friction) and the Coulomb threshold are relevant. In addition, frictional effects may lead to a change from overshoot to a monotonous increase of penetration depth with time, suggesting that friction plays an important role in determining the forces that an intruder experiences during impact.

(3) The analysis of the force field in the granular material confirms a strong influence of tangential forces. In addition, our results are consistent with a transition from a hyperbolic to an elastic type of force propagation through the granular matter. For example, a more pronounced pressure dip may be seen below the point of impact for a kinetic friction type of interaction between the granular particles, compared to the static friction.

(4) The analysis of the displacement field shows stronger affine and nonaffine deformation for systems of particles interacting via the kinetic friction model, suggesting that increased mobility of the particles when static friction is not included is responsible for larger penetration depths.

To further illustrate the influence of friction and of elastic damping on the dynamics, we discuss briefly the evolution of the energy in the system consisting of the intruder and granular

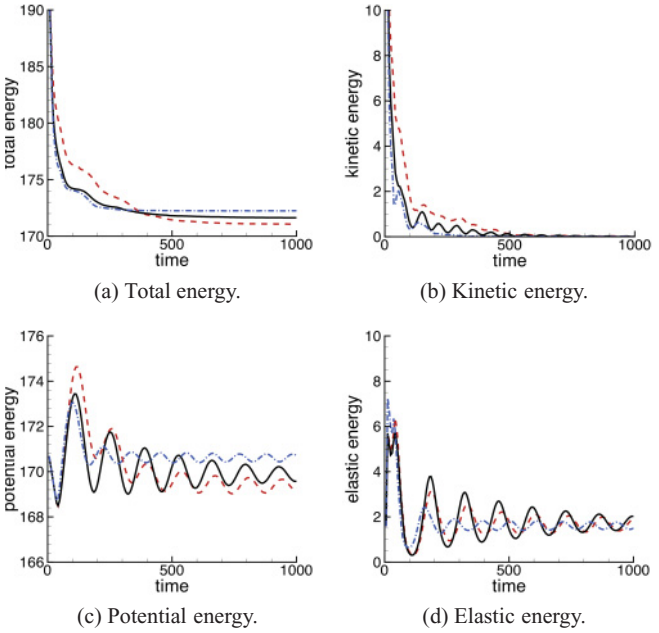

(a) Total energy. (b) Kinetic energy.
(c) Potential energy. (d) Elastic energy.

FIG. 28. (Color online) Combined energy of the intruder and granular particles during impact for three systems characterized by different frictional properties; penetration depth vs time is shown in Fig. 6. Here we show the results for $\mu = 0$ (red dashed line); $\mu = 0.5$, $k_t = 0.0$ (black solid line), and $\mu = 0.5$, $k_t = 0.8$ (blue dash-dotted line). The parameters are as in Fig. 6.

particles. Figure 28 shows the total, kinetic, potential, and elastic energies as a function of time for combined intruder and granular particles system. For brevity, only the results obtained for polydisperse systems are shown since the results for monodisperse ones are similar. The total energy, which is the sum of the kinetic, potential, and elastic energies for the complete system (granular particles and intruder) shows a monotonous decrease and illustrates faster loss of energy for the systems with friction (kinetic or static). Figure 28(b) shows that kinetic energy is lost very quickly, again faster in the case of frictional systems. Figures 28(c) and 28(d) show that the exchange of energy between potential and elastic components persists for much longer times, although both the intruder and the granular particles are essentially at rest, as can be seen from the kinetic energy plot [Fig. 28(b)].

We conclude that the energy evolution is similar for the three types of systems considered here, with the differences between static and kinetic friction models being surprisingly minor. Therefore, energy balance on its own does not provide a complete picture since, as can be seen clearly in, for example, Fig. 6, static friction leads to a significant decrease in the penetration depth. It is necessary to go beyond energy balance and explore the structure of the force field and dynamical response of granular media to gain a better understanding of the interaction of an intruder with a granular system, and its consequences on the final penetration depth.

In this work we have concentrated only on relatively shallow impacts, where the final penetration depth is comparable to or smaller than the intruder's size. Future work will analyze deeper penetration, as well as directly compare computational results with two-dimensional experiments. In addition, it is of

importance to extend the simulations to three dimensions to be able to compare with the much wider range of experimental results, and quantify the influence of dimensionality on the results. This work is currently ongoing.

ACKNOWLEDGMENTS

We thank Konstantin Mischaikow and Miroslav Kramar for introducing us to the topic of computational topology. This work was supported by DTRA Grant 1-10-1-0021 and NSF Grant No. DMS-0835611.

APPENDIX: COMPARISON TO EFFECTIVE MODELS AND EXPERIMENTAL RESULTS

A simple model for the force describing interactions between an intruder and granular material can be outlined as follows (see, e.g., [7,8,10]). The total force on the intruder includes gravity, and the force due to interaction with the granular material. The interaction force may be considered as a separable function of two variables, $(y(t),u(t))$, where $y(t)$ is the time dependent position of the intruder and $u(t)$ is its time-dependent velocity

$$\sum F = Mg + F_d(y) + F_v(u). \tag{A1}$$

Here M is the mass of the intruder and the positive y directions points in the direction of gravity (for simplicity, we also use y to refer to the time-dependent depth of the intruder). It should be noted here that there is a strong assumption that this separation can actually be done, which is not clear *a priori*. However, assuming that this separated model is appropriate, one can proceed to discuss the origin of the force terms. The depth-dependent force $F_d(y)$ may be taken to be a result of resistance by the granular material to impact, which is present even for vanishing velocity. This force is commonly considered to be due to friction, although it was recently observed to be present even if frictional effects were absent [13]. As reported in the literature [7,8,10,13], by exploring an analogy with hydrostatic forces which govern propagation though a Newtonian fluid, $F_d(y)$ is expected to vary linearly with y, $F_d \propto y$ for large y, with more complicated behavior expected for smaller y [10]. The velocity dependent force $F_v(u)$ is the inertial drag force, required to push away the particles in front of the intruder. For an intruder of diameter D_i and having velocity u, a simple argument [10] suggests that this component of the force scales as $F_v \propto u^2$, although one can also find evidence for linear scaling $F \propto u$ [3,8].

To examine the depth dependent force $F_d(y)$, we consider a number of different impact velocities v and we find the intruder's acceleration as a function of y, at fixed u. For brevity, here we discuss only impacts on polydisperse, disordered systems. Figures 29(a), 29(c), and 29(e) show the results obtained for three systems: Coulomb threshold $\mu = 0$ (frictionless), and $\mu = 0.5$ with kinetic $k_t = 0$ and static $k_t = 0.8$ friction. For the frictionless case, shown in Fig. 29(a), we find monotonously increasing $a(h)$, with a dependence which can be described reasonably well by a linear fit, consistent with several previous studies [8,13]. Friction, however, leads to modifications not only of the linearity, but also of *monotonicity* of the $a(y)$ dependence, as illustrated in

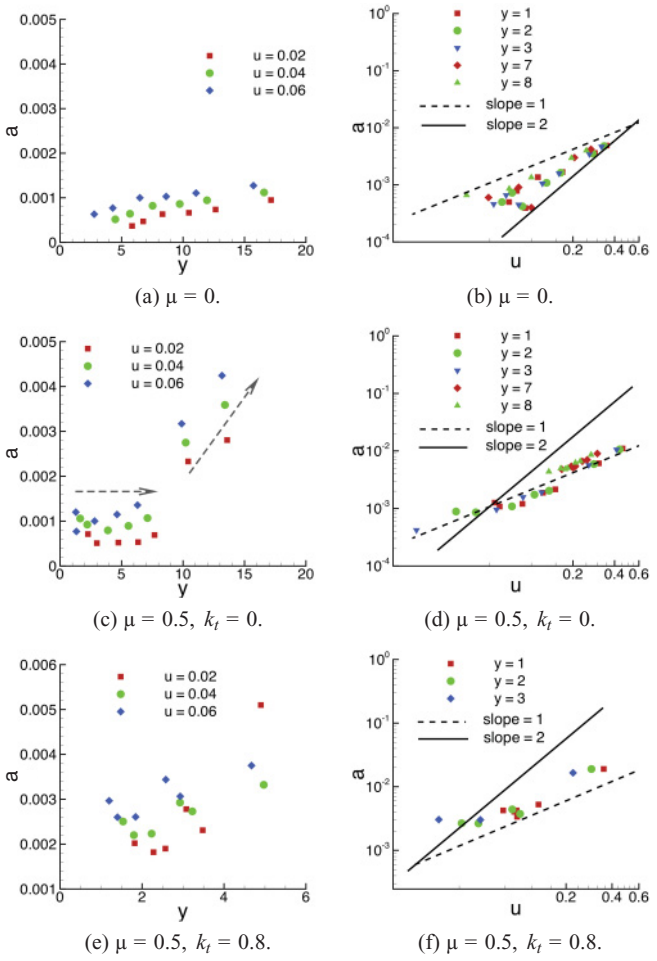

(a) $\mu = 0$. (b) $\mu = 0$.

(c) $\mu = 0.5$, $k_t = 0$. (d) $\mu = 0.5$, $k_t = 0$.

(e) $\mu = 0.5$, $k_t = 0.8$. (f) $\mu = 0.5$, $k_t = 0.8$.

FIG. 29. (Color online) Intruder's acceleration vs its time-dependent depth $y(t)$ and time-dependent velocity $u(t)$. The impact velocities are $v = 0.05$, $v = 0.1$, $v = 0.2$, $v = 0.3$, $v = 0.4$, $v = 0.7$, and $v = 1.0$. The parameters that are not varied are as in Fig. 2.

Figs. 29(c) and 29(e), where kinetic and static friction were considered, respectively. The deviation from monotonicity is particularly obvious for small y, as expected based on the arguments given in [10]. Therefore we find that the dependence of the intruder's acceleration on time-dependent penetration depth $y(t)$ is strongly influenced by the frictional properties of the granular material.

Let us now consider the dependence of the intruder's acceleration on its time-dependent velocity u. To do so we again consider different initial velocities v and find $a(u)$ for fixed y. Figures 29(b), 29(d), and 29(e) show the results for the three different friction cases. We extract $a(u)$ for relatively small y, where the acceleration is relatively large, in order to decrease the scatter of the results. Note that for the static friction case we could extract accelerations only for y between 1 and 3 since the final penetration depth is small here.

First, we note that Figs. 29(b), 29(d), and 29(e) do not show any obvious y dependence. That is, for fixed u, a does not appear to depend on y. By comparison of the results we see however that there is a strong influence of friction. Only the frictionless and kinetic friction lead to approximate power-law scaling $a \propto u^k$, at least for the parameters considered here. As

seen in Figs. 29(b) and 29(d), the fitting exponent k is smaller than the proposed value $k = 2$ [7,10,13]; for the frictionless case we find a best fit with $k \approx 1.4$, and for the kinetic friction case we find $k \approx 1$ [3]. From the frictionless results shown in Fig. 29(b) it does appear, however, that the slope increases with the depth y, suggesting that different scaling may be found at different depths. We conjecture that the parameters and penetration depths considered here belong to the "intermediate range" where there is no precisely defined scaling regime [8].

Clearly more work is needed to understand precisely the nature of the forces determining impact dynamics, and their dependence on the quantities such as the velocity of intruder or its depth. In any case, at least from the point of view of a comparison with physical experiments carried out, necessarily with frictional particles, the most relevant conclusion is that the speed dependence of the force on the intruder may be influenced strongly by the friction model for intergranular forces. As pointed out [10], this aspect of the problem is complicated by the fact that most particle interaction laws include velocity-dependent frictional damping, which may prevent us from reaching generic answers regarding the speed dependence of the force on an intruder.

Finally, we briefly compare our simulations with the available experimental results for the dependence of penetration on the falling distance. In the experiments of Durian *et al.* [7], it was found that the final penetration depth dependence can be well fitted by $\bar{D} \propto H^{1/3}$, where $H = h + y$, and h is the falling distance before impact. Other investigators have found somewhat different results, suggesting $\bar{D} \propto v$ [4,8]. We have already briefly mentioned scaling of $\bar{D}$ with v, see Fig. 8, where we saw that approximately $\bar{D} \propto v$.

Figure 30 shows $\bar{D}$ for a polydisperse, disordered system [Fig. 30(a)], and for a monodisperse, ordered system [Fig. 30(b)]. We find that for an impact on a polydisperse system $\bar{D}$ can be fitted reasonably well by a power law using an exponent which is close (although typically a bit smaller) than $1/3$. The main deviation occurs for very small values of H, for which the penetration depth is also very small. However, the quality of the fit is not sufficient to distinguish between $\bar{D} \propto H^{1/3}$ scaling shown here, or $\bar{D} \propto v$, suggested by Fig. 8. We do not find a significant influence of friction model here, aside from significantly smaller penetration depths for the frictional cases.

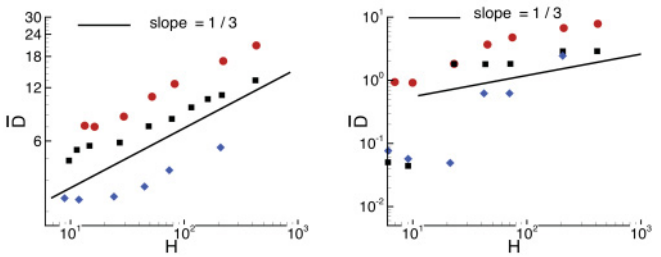

(a) $r = 0.2$. (b) $r = 0.0$.

FIG. 30. (Color online) Intruder's final penetration depth $\bar{D}$ vs $H = h + y$, where h is the falling distance. Here we show $\mu = 0.0$ (red circles), $\mu = 0.5$, $k_t = 0$ (black squares), and $\mu = 0.5$, $k_t = 0.8$ (blue diamonds). The parameters that are not varied are as in Fig. 2.

For impacts on a monodisperse, ordered system, we find that the results are significantly different, in particular for the frictional cases. There is no obvious scaling of the penetration depth with the total falling distance H. This result underscores the fact that an ordered granular microstructure can have a significant influence on the penetration process. Future research should show the generality of this conclusion.

[1] J. Poncelet, *Course de Mécanique Industrielle* (Paris, 1829).
[2] J. S. Uehara, M. A. Ambroso, R. P. Ojha, and D. J. Durian, Phys. Rev. Lett. **90**, 194301 (2003).
[3] M. P. Ciamarra, A. H. Lara, A. T. Lee, D. I. Goldman, I. Vishik, and H. L. Swinney, Phys. Rev. Lett. **92**, 194301 (2004).
[4] J. R. de Bruyn and A. M. Walsh, Can. J. Phys. **82**, 439 (2004).
[5] M. A. Ambroso, C. R. Santore, A. R. Abate, and D. J. Durian, Phys. Rev. E **71**, 051305 (2005).
[6] M. A. Ambroso, R. D. Kamien, and D. J. Durian, Phys. Rev. E **72**, 041305 (2005).
[7] H. Katsuragi and D. J. Durian, Nat. Phys. **3**, 420 (2007).
[8] D. I. Goldman and P. Umbanhowar, Phys. Rev. E **77**, 021308 (2008).
[9] P. Umbanhowar and D. I. Goldman, Phys. Rev. E **82**, 010301 (2010).
[10] L. S. Tsimring and D. Volfson, in *Powders and Grains*, edited by R. Garcia-Rojo, H. J. Hermmann, and S. McNamara (A. A. Balkema, Leiden, 2005), p. 1215.
[11] M. Nishida, K. Tanaka, and Y. Matsumoto, JSME Int. J. Ser. A **47**, 438 (2004).
[12] F. Bourrier, F. Nicot, and F. Darve, Granul. Matter **10**, 415 (2008).
[13] A. Seguin, Y. Bertho, P. Gondret, and J. Crassous, Europhys. Lett. **88**, 44002 (2009).
[14] L. Kondic, Phys. Rev. E **60**, 751 (1999).
[15] J. Schäfer, S. Dippel, and D. E. Wolf, J. Phys. I France **6**, 5 (1996).
[16] J. Geng, R. P. Behringer, G. Reydellet, and E. Clément, Physica D **182**, 274 (2003).
[17] P. A. Cundall and O. D. L. Strack, Géotechnique **29**, 47 (1979).
[18] L. Brendel and S. Dippel, in *Physics of Dry Granular Media*, edited by H. J. Herrmann, J.-P. Hovi, and S. Luding (Kluwer Academic, Dordrecht, Netherlands, 1998), p. 313.
[19] M. Lätzel, Ph.D. thesis, Universität Stuttgart, Stuttgart, Germany, 2003.
[20] C. Goldenberg and I. Goldhirsch, Nature (London) **435**, 188 (2005).
[21] K. Daniels, J. Coppock, and R. Behringer, Chaos **14**, S4 (2004).
[22] K. A. Newhall and D. J. Durian, Phys. Rev. E **68**, 060301 (2003).
[23] M. B. Stone, D. P. Bernstein, R. Barry, M. D. Pelc, Y.-K. Tsui, and P. Schiffer, Nature (London) **427**, 503 (2004).
[24] A. Seguin, Y. Bertho, and P. Gondret, Phys. Rev. E **78**, 010301 (2008).

[25] S. von Kann, S. Joubaud, G. A. Caballero-Robledo, D. Lohse, and D. van der Meer, Phys. Rev. E **81**, 041306 (2010).
[26] E. L. Nelson, H. Katsuragi, P. Mayor, and D. J. Durian, Phys. Rev. Lett. **101**, 068001 (2008).
[27] L. Kondic, O. M. Dybenko, and R. P. Behringer, Phys. Rev. E **79**, 041304 (2009).
[28] See Supplemental Material at http://link.aps.org/supplemental/10.1103/PhysRevE.85.011305 for animations of the force field during impact.
[29] L. Silbert, Granul. Matter **12**, 135 (2010).
[30] A. Cakir and L. Silbert, J. Stat. Phys. (2011) P08005.
[31] C. Goldenberg and I. Goldhirsch, Phys. Rev. E **77**, 041303 (2008).
[32] T. Kacynksi, K. Mischaikow, and M. Mrozek, *Computational Homology* (Springer, New York, 2004).
[33] K. Mischaikow, Computational Homology Project, http://chomp.rutgers.edu/.
[34] F. Radjai, M. Jean, J. J. Moreau, and S. Roux, Phys. Rev. Lett. **77**, 274 (1996).
[35] M. L. Falk and J. S. Langer, Phys. Rev. E **57**, 7192 (1998).